Magnetic excitations in the longitudinally polarized antiferromagnetic phase of praseodymium

Jens Jensen
Physics Laboratory, H. C. Ørsted Institute, DK-2100 Copenhagen Ø, Denmark

Keith A. McEwen* and William G. Stirling
Institut Laue-Langevin, 156X, 38042 Grenoble Cedex, France

(Received 24 December 1985; revised manuscript received 20 November 1986)

In the ordered phase of Pr, which can be induced by the application of a uniaxial pressure, the length of the moments is modulated sinusoidally with a period incommensurate with the lattice. A comprehensive theory has been developed to describe the ground-state properties and the excitation spectrum of this antiferromagnetic phase. Numerical results, based on parameters determined from paramagnetic Pr, are compared with neutron scattering experiments. In order to account for linewidth effects several mechanisms which broaden the excitations are considered. Contributions due to the incommensurate modulation are included but are found to be small. To first order in the high-density $(1/z)$ expansion, the effects of the single-site fluctuations vanish exponentially in the zero-temperature limit. The second-order contributions, derived in the present paper, are then the leading-order terms at low temperatures and are found to be important. Additionally, the scattering against electron-hole pair excitations of the conduction electrons is treated by incorporating it directly in the $1/z$ expansion. The theory yields a reasonably realistic description of the neutron scattering results. It can be concluded that the phason mode, near the ordering wave vector, is a damped diffusive mode. The principal remaining puzzle, the quasielastic peak not centered at the ordering wave vector, is tentatively ascribed to heavy-fermion behavior in Pr.

I. INTRODUCTION

Most of the magnetic properties of the light rare-earth metal praseodymium in its paramagnetic phase are well understood.[1] The $4f^2, J=4$ ions of the double hexagonal close-packed (dhcp) structure experience crystal fields with either hexagonal or (nearly) cubic symmetry and both the crystal-field ground states are singlets with the dipolar-excited states lying about 3.5 and 8.4 meV above the ground states of the hexagonal and the cubic ions, respectively. Mainly because of the larger crystal-field splitting on the cubic sites, the moments on these sites only have weak effects on the low-frequency properties. The two-ion coupling is about 92% of the critical value required to induce long-range magnetic ordering. The magnetoelastic coupling between the crystal-field splittings and an orthorhombic distortion of the hexagonal planes is large. The presence of this coupling enables the threshold value for inducing magnetic ordering to be reduced by the application of a uniaxial pressure in the basal plane. Since the first report[2] of the observation of the pressure-induced magnetic phase in Pr, a number of neutron scattering experiments have been performed to investigate both the elastic and inelastic magnetic response in this ordered phase. Sections of the most informative results have been published in various places.[3–6] We are not attempting to give here a full account of these experiments, which is reserved for a future publication, but rather we incorporate those results, a few of which are hitherto unpublished, which are of importance for our arguments.

In the present paper, we develop a theory adequate for describing most of the phenomena observed in the ordered phase of Pr. The theory is confronted directly with experimental results, and in this comparison we use only parameters already known from the experiments[1] on paramagnetic Pr. In the next section we consider the ground-state properties of Pr, when the crystal is subjected to a uniaxial pressure. In Sec. III we discuss the excitation spectrum of the ordered phase. The emphasis is laid on the excitations, which have the same symmetry properties as the ordered moments, as these are most noticeably modified in comparison with the paramagnetic excitations. In this part of the analysis we utilize the random-phase approximation (RPA) for simplicity. However, we include effects due to the infinite size of the coupling matrix, occurring because the modulation of the moments is incommensurate. In Sec. IV we go beyond the RPA in a study of the lifetime of the "excitons." In the high-density $1/z$ expansion (z denotes the number of nearest neighbors) the leading-order contribution is due to the scattering against single-site fluctuations, as first considered by Bak[7] for the case of paramagnetic Pr. Here we extend these calculations by including the first-order contributions due to the fluctuating moments, but we also find it necessary to proceed to next order in $1/z$, in order to calculate the dynamical behavior at low temperatures. Finally, we note that the excitons are additionally scattered by electron-hole pair excitations of the conduction electrons. This scattering mechanism can be included in a straightforward manner in the $1/z$ expansion. The results obtained are summarized in the conclusion, Sec. V.

II. THE GROUND STATE OF Pr

A detailed discussion of the Hamiltonian describing the angular momentum system of the $4f$ electrons in Pr metal is given in Ref. 1. Except where specifically stated, we shall henceforth only be concerned with the ions at the hexagonal sites. The crystal-field part of the Hamiltonian leads to the ground state $|J_z=0\rangle$ and with the $|\pm1\rangle$ doublet as the lowest excited state about 3.5 meV above the ground state (the x, y, and z axes are defined to be along, respectively, the real-space a, b, and c axes of the hexagonal lattice). The application of a uniaxial pressure in the basal plane lifts the degeneracy of the $|\pm1\rangle$ doublet. As discussed in Ref. 1 the magnetoelastic coupling parameter, which determines the splitting, is well established, and in Fig. 1 we show the calculated energies relative to the ground state of the two crystal-field levels and of the nearby $|3_s\rangle$ state, as functions of the applied pressure. Starting from the ground state the levels are numbered 0, 1, 2, etc., with the corresponding excitation energies denoted by $\Delta_1=E_1-E_0$, etc. The remaining five levels, which are not included in the figure, are estimated to lie at much higher energies ($\gtrsim 7$ meV). The magnetoelastic quadrupole term introduced in the Hamiltonian for Pr under pressure mixes the different state vectors slightly. Consequently, M_1 defined as the numerical value of the matrix element of J_y between the ground state and the lowest excited state becomes slightly larger than $|\langle 1_a|J_y|0\rangle|=\sqrt{10}$, leading to $M_1\cong 1.026\sqrt{10}$ at 1 kbar.

In the molecular-field (MF) approximation the total ground state is the product state of the nonmagnetic $|0\rangle$ singlets. The presence of an interaction between the different angular momenta, $\mathcal{J}(ij)$, implies that the crystal-field excitations are changed into collective dispersive modes, i.e., the magnetic excitons. If the two-ion coupling is sufficiently large the nonmagnetic MF ground state becomes unstable below the temperature at which the RPA energy of the lowest-lying exciton vanishes (a so-called "soft-mode transition"). At zero pressure the lowest-lying excitations in Pr are the longitudinally polarized optic modes propagating along ΓM which have a broad minimum around the wave vector $0.12\tau_{100}$. In the zero-temperature limit the minimum excitation energy is 1.0 meV, and it would vanish if the exchange coupling were increased by about 8%. With a pressure applied along the x axis the minimum in the dispersion relation occurs for the excitons propagating in the y direction (i.e., ΓM perpendicular to the pressure axis). These remain pure transverse or longitudinal modes, and the RPA energy[1] of the optical, longitutional modes may be written ($\mathbf{q}||\hat{\mathbf{y}}$)

$$\varepsilon_l(\mathbf{q})=[\Delta_1(\Delta_1-2n_{01}M_1^2\mathcal{J}(\mathbf{q}))]^{1/2}\,, \tag{1}$$

with $\mathcal{J}(\mathbf{q})$ defined as the (effective) exchange parameter for these modes. $n_{01}=n_0-n_1$ is the population difference between the ground state and the first excited state of the MF Hamiltonian. When the uniaxial pressure is ap-

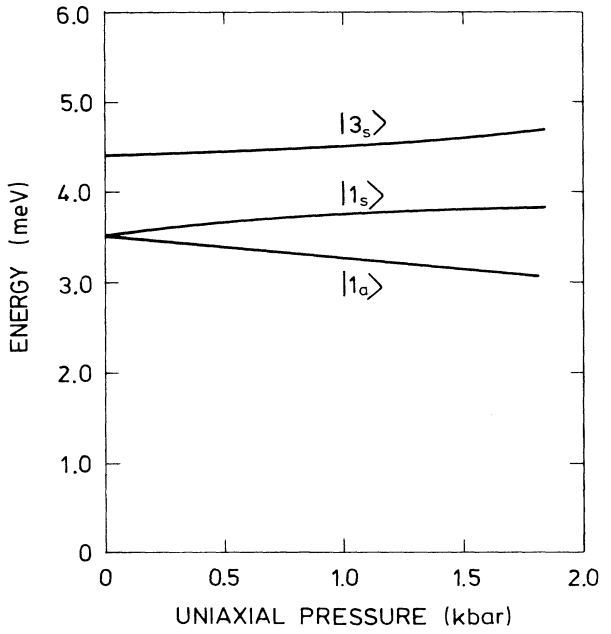

FIG. 1. The crystal-field splittings of the lowest levels of the hexagonal ions in Pr. The energies relative to the ground state are calculated, using the parameters given by Houmann *et al.* (Ref. 1), as functions of a uniaxial pressure applied in the a direction (x axis). The state-vector designation of the levels is the one at small values of the pressure.

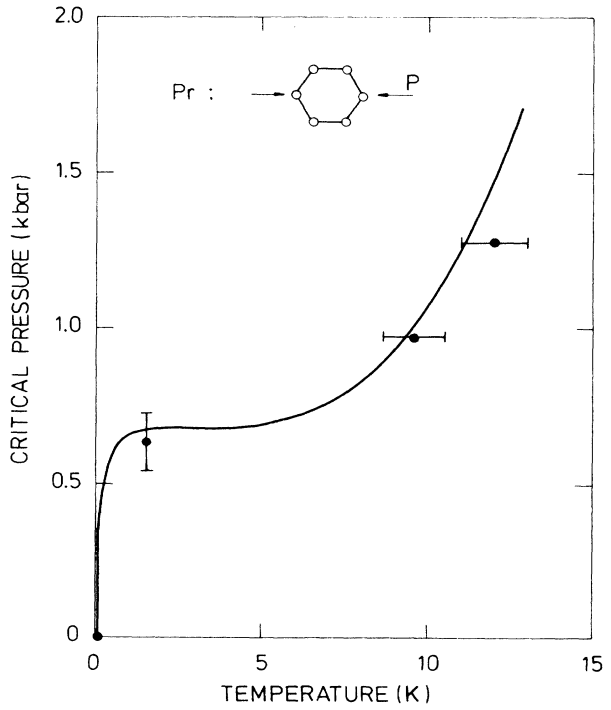

FIG. 2. T_N in Pr calculated as a function of the uniaxial pressure, using the MF model of Houmann *et al.* (Ref. 1). Solid circles show the results obtained from neutron-diffraction measurements of McEwen, Stirling, and Vettier (Refs. 3 and 4).

plied along the x axis, $\varepsilon_l(\mathbf{q})$ shifts downwards and the minimum energy, at $\mathbf{q}=\mathbf{Q}$, may be reduced to zero, at a finite temperature T_N, when the pressure exceeds a critical value, which is calculated to be about 0.7 kbar. Below T_N, Pr is magnetically ordered in a structure, which, at least close to T_N, is that characterizing the soft mode. Figure 2 shows T_N calculated as a function of pressure and compared with the experimental results of the neutron-diffraction measurements.[2-6] The hyperfine coupling to the nuclear spins has been included in the calculation and is of importance below ~ 1 K. This interaction produces a cooperative transition in the electron-nuclear spin system at about 50 mK at zero applied pressure.[6,8-10] It is important to note that the extraction of T_N from the experimental data is complicated by the presence of strong critical scattering. The results of Fig. 2 represent the temperatures where the linear variation of the magnetic satellite intensities found in the ordered phase somewhat below T_N extrapolates to zero. The threshold value of about 0.63 kbar at 1.5 K is obtained by considering the similar variation of the intensities with pressure. In the determination of T_N all the crystal-field levels of the hexagonal ions are included; however, in the following we neglect the higher-lying levels left out from Fig. 1. This is a fair approximation in the low-temperature regime with which we shall be concerned, but we shall comment on the corrections due to the higher-lying levels.

The moment induced on the cubic sites below T_N is only about one tenth of the moment on the hexagonal sites, and in most respects the presence of the cubic moments is accounted for by the introduction of an effective coupling within the hexagonal lattice (see also Ref. 1). The moments of the hexagonal ions are directed along the b axis perpendicular to the pressure axis. The length of the moments is linearly modulated with a wave vector $\mathbf{Q}$:

$$\langle J_{y,i}\rangle = M_1[\,\sigma_1\cos(\mathbf{Q}\cdot\mathbf{R}_i+u_1) + \sigma_3\cos(3\mathbf{Q}\cdot\mathbf{R}_i+u_3)+\cdots\,] \quad (2)$$

anticipating the possibility of odd higher harmonics (σ_3, σ_5, etc.). The diffraction measurements[3,4] indicate also a perpendicular component of the moments, $\langle J_x\rangle$, of about one tenth of $\langle J_y\rangle$ corresponding to a small rotation of $\langle\mathbf{J}\rangle$ away from the y axis (the possibility of an elliptically polarization of the moments can be left out because of the large anisotropy of the exchange coupling). The possible rotation of $\langle\mathbf{J}\rangle$ is expected to be accompanied by a simultaneous rotation of $\mathbf{Q}$ (the two angles of rotation need not be the same), but such rotation has not been resolved in the present system. A rotation of both $\langle\mathbf{J}\rangle$ and $\mathbf{Q}$ has been observed[11,12] in the equivalent system Nd, and indications for a rotation of $\mathbf{Q}$ away from the ΓM direction have been found[10] in unstressed Pr in the mK range. However, the rotation of $\langle\mathbf{J}\rangle$ and/or of $\mathbf{Q}$ in these latter systems is probably a consequence of a double-$\mathbf{Q}$ or a triple-$\mathbf{Q}$ ordering of the moments. An analysis of the MF model for Pr (see also Forgan[13]) shows that the most stable ordered configuration at zero pressure is the double-$\mathbf{Q}$ structure, modified by small rotations of $\langle\mathbf{J}\rangle$ and $\mathbf{Q}$ around the c axis away from the two ΓM directions involved. In the MF approximation the energy differences between the single-$\mathbf{Q}$ and the multiple-$\mathbf{Q}$ structures are small (they vanish at T_N). The application of the uniaxial pressure clearly favors the single-$\mathbf{Q}$ ordering described by (2), and the MF model indicates that this structure becomes the most stable one when the pressure exceeds only about 100 bars when considering $\sigma_1=0.4$. Because this pressure is a factor of 10 smaller than required for obtaining $\sigma_1\cong 0.4$, the MF model indicates that a multiple-$\mathbf{Q}$ ordering of the moments in the present system is unlikely. In the experimental setup any tendency towards plastic deformations of the sample was constrained geometrically by the pressure rig. This may, however, create small domains in the crystal where the direction of the pressure axis deviates from the x axis [for instance, connected to the slip planes which make angles $\pm 30°$ with the (yz) plane] and thereby inducing a finite $\langle J_x\rangle$ component. A definitive clarification of these questions awaits further experimental investigations. Fortunately, the possible components of $\langle\mathbf{J}\rangle$ or $\mathbf{Q}$ along the x axis are so small that they should be of no significance in the present analysis.

Experimentally, $\mathbf{Q}$ in Eq. (2) is found to be close to one eighth of the reciprocal-lattice vector τ_{100}. It depends slightly on temperature and pressure,[4] for instance at 970 bars $\mathbf{Q}$ is $0.120\tau_{100}$ at T_N and very nearly $0.125\tau_{100}$ at zero temperature. Although $\mathbf{Q}$ in certain regimes might be a rational fraction of a reciprocal-lattice vector we proceed considering the case of an incommensurate ordering of the moments. The molecular field acting on the ith

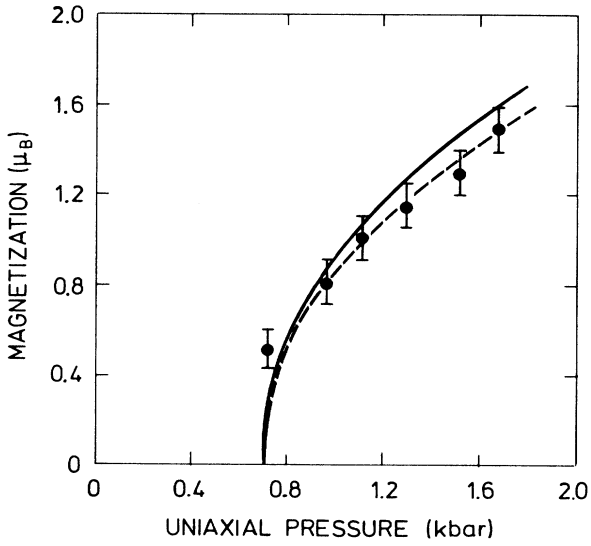

FIG. 3. Experimental measurements of the first harmonic of the magnetization in Pr, deduced from the integrated intensities of the (Q01) diffraction peaks at 1.5 K as a function of the uniaxial pressure. There is still an appreciable peak intensity left below ~ 0.63 kbars, which we ascribe to strong critical fluctuations and not to a true long-range ordering of the system. The dashed line is the result obtained using the effective $S=1$ model, whereas the solid line includes the effects of all the $J=4$ levels.

site leads to the ground state $|g_i\rangle=\cos\theta_i|0\rangle+\sin\theta_i|1\rangle$, and hence

$$\langle J_{y,i}\rangle=M_1 n_{01}(i)\sin(2\theta_i)\ , \tag{3}$$

and the MF Hamiltonian is diagonal when

$$\tan(2\theta_i)=\frac{2M_1^2}{\Delta_1}[\sigma_1\mathcal{J}(\mathbf{Q})\cos(\mathbf{Q}\cdot\mathbf{R}_i+u_1)+\sigma_3\mathcal{J}(3\mathbf{Q})\cos(3\mathbf{Q}\cdot\mathbf{R}_i+u_3)+\cdots]\ . \tag{4}$$

The Eqs. (2)—(4) can be solved utilizing $\theta_i\propto\sigma_1$ as an expansion parameter, and their solution is presented in the Appendix. The first harmonic of the magnetization, $m_1=g\mu_B M_1\sigma_1$, per hexagonal ion, has been calculated as a function of the uniaxial pressure in the zero-temperature limit, both with the use of the effective $S=1$ model, Eq. (A6), and with all the MF levels included, and the results are compared with neutron-diffraction results in Fig. 3. Further, the third harmonic is determined relatively by $m_3/m_1=\frac{1}{6}(1-2/\xi_3)\xi_1$ (ξ_n are defined in the Appendix), and is calculated to be 0.024, at 970 bars and $T=0$, in agreement with the measured value of ~0.02. The comparisons in the Figs. 2 and 3 show that the MF Hamiltonian established in Ref. 1 accounts very well for the ground-state properties of Pr under uniaxial pressure.

III. RPA EXCITATIONS IN THE INCOMMENSURATE PHASE

We shall proceed to consider the excitations in the ordered phase, and we shall be almost exclusively concerned with the longitudinal (optic) modes which propagate parallel with Q. In the RPA the two-site Green's functions are determined self-consistently by

$$G(ij,\omega)=g_i^0(\omega)\delta_{ij}+\sum_{j'}g_i^0(\omega)\mathcal{J}(ij')G(j'j,\omega)\ , \tag{5}$$

where $g_i^0(\omega)$ is the single-site Green's function. In general, these quantities are 3×3 matrices; however, the longitudinal yy component stays diagonal in the present case. The "noninteracting" yy component is

$$g_j^0(\omega)=\frac{2\Delta_1(j)n_{01}(j)M_1^2\cos^2(2\theta_j)}{\Delta_1^2(j)-\omega^2}+\frac{i\epsilon}{\omega+i\epsilon}\beta(n_0+n_1-n_{01}^2)_j M_1^2\sin^2(2\theta_j),\quad \epsilon\to0+\ . \tag{6}$$

First, we notice that $g_j^0(\omega)$ includes both an inelastic and an elastic term, and that the elastic contribution vanishes in both the limits $T\to0$ and $T\to T_N$ ($\propto\sigma_1^2\beta e^{-\beta\Delta}\ll1$). Secondly, due to the modulation of the lengths of the moments $g_j^0(\omega)$ depends on j, which means that (5) cannot be diagonalized by a Fourier transformation. Defining the double-Fourier-transformed Green's functions

$$G_n(\mathbf{q},\omega)=\frac{1}{N}\sum_{i,j}G(ij,\omega)e^{i\mathbf{q}\cdot(\mathbf{R}_i-\mathbf{R}_j)}e^{in\mathbf{Q}\cdot\mathbf{R}_i}\ . \tag{7}$$

Then the coupled equations of motion for determining $G_{2n}(\mathbf{q},\omega)$ are

$$[E_{2n}(\mathbf{q})-\omega^2]G_{2n}(\mathbf{q},\omega)+V_{2n+2}(\mathbf{q})G_{2n+2}(\mathbf{q},\omega)+V_{2n-2}(\mathbf{q})G_{2n-2}(\mathbf{q},\omega)=2\Delta_1\bar{n}_{01}M_1^2[\lambda_2\delta_{n,0}+\lambda_4(\delta_{n,1}+\delta_{n,-1})]\ , \tag{8}$$

where $n=0,\pm1,\pm2,\ldots$, and the expressions for the parameters appearing here can be found in the Appendix. The off-diagonal couplings $V_{2n\pm2}(\mathbf{q})$ and λ_4 are of the order $\xi_1\cong\frac{1}{4}\sigma_1^2$, but we have neglected the couplings between G_{2n} and $G_{2n\pm2p}$, with $p=2,3,\ldots$. These are of the order $(\xi_1)^p$, and thus only contribute to the eigenvalues in the order $(\xi_1)^{2p}$. We note that the couplings with $p=4$ actually give corrections of the order ξ_1^4, because $2p\mathbf{Q}$ in this case is near to being a reciprocal-lattice vector.

The quantity in (8) which we need to calculate is $G_0(\mathbf{q},\omega)$, as the neutron inelastic scattering cross section is proportional to the correlation function

$$S(\mathbf{q},\omega)=\frac{1}{\pi}\frac{1}{1-e^{-\beta\omega}}\mathrm{Im}G_0(\mathbf{q},\omega)\ . \tag{9}$$

In the incommensurate case the coupling matrix in (8) is of infinite extension. A perturbative decoupling leads to poles lying on the real axis (in RPA), whereas the infinite extension of the coupling matrix implies that the excitations have a nonzero linewidth. We have estimated the importance of this nonperturbative change in the behavior by considering

$$G_0(\mathbf{q},\omega)=G_0=2\Delta_1\bar{n}_{01}M_1^2\frac{\lambda_2-\lambda_4(Z_2+Z_{-2})}{E_0-V_0(Z_2+Z_{-2})-\omega^2} \tag{10a}$$

(we suppress the arguments $\mathbf{q}$ and ω), where Z_2 is determined from (8) in terms of the infinite continued fraction

$$Z_{2n}=\frac{V_{2n}}{E_{2n}-\omega^2-V_{2n}Z_{2n+2}},\quad n=1,2,\ldots, \tag{10b}$$

and Z_{-2} is given similarly by changing the sign of the indices in (10b), A simple perturbative approach consists in assuming $Z_{\pm2n}$ in the expressions for $Z_{\pm2}$ to be zero for a certain value of n (≥2). Here, we replace instead this $Z_{\pm2n}$ by its mean value

$$\langle Z\rangle=\frac{1}{p}(Z_2+Z_4+\cdots+Z_{2p})_{p\to\infty}\ .$$

With $\mathbf{Q}$ being incommensurate, this is the same as the average of $Z_{\pm2n}=Z_{\pm2n}(\mathbf{q},\omega)$ with respect to $q_{\|}=\mathbf{q}\cdot\mathbf{Q}/|\mathbf{Q}|$, giving the self-consistent equation $\langle Z\rangle=\langle Z_{\pm2}(\mathbf{q},\omega)\rangle_{q_{\|}}$. A useful solution is found if $G_0(\mathbf{q},\omega)$ exhibits a stationary behavior, by which we mean that $G_0(\mathbf{q},\omega)$ should be independent of the value of n chosen for the substitution of $Z_{\pm2n}$ with $\langle Z\rangle$, when n becomes sufficiently large. Although it might not be easy to decide whether this condition is actually fulfilled, the results using this procedure[14] compare very well with calculations of Ziman and Lindgård.[15] These authors use a dif-

ferent approach with models corresponding to the present one when ξ_1 is of the order of unity. The consistency of the results obtained by the two different procedures[14] in the "strong coupling" limit supports the validity of the results obtained in the case here where ξ_1 is small ($\xi_1 < 0.1$). We conclude that the linewidth, due to the infinite range of the coupling matrix, is negligible, since it is at least 1 order of magnitude smaller than the excitation energies. We may phrase this differently by stating that whether $\mathbf{Q}$ is incommensurate or not is of no importance for the linewidth of the excitations.

The effects of the off-diagonal terms in (8) on the excitation energies are, in general, of the order of ξ_1^2, except in the cases of degeneracy: $E_0(\mathbf{q}) = E_{\pm 2}(\mathbf{q}) = E_0(\mathbf{q} \pm 2\mathbf{Q})$. The most significant occasion is when $\mathbf{q} = \pm\mathbf{Q}$. The coupling of the modes at $\mathbf{Q}$ and $-\mathbf{Q}$ leads to an amplitude and a phason mode, i.e., an in-phase and an out-of-phase modulation of the lengths of the moments, respectively. The excitation energies at $\pm\mathbf{Q}$ are found to be given by

$$\omega_p^2 = \gamma \left[1 + \frac{13}{6}\xi_1 + \frac{2}{3}\frac{\xi_1}{\xi_3} \right] \Delta_1^2 \tag{11a}$$

for the phason mode, and

$$\omega_A^2 = 3\xi_1 \left[1 + \frac{4}{3}\xi_1 + \frac{1}{3}\frac{\xi_1}{\xi_3} + \frac{1}{3}\gamma \right] \Delta_1^2 + \omega_p^2 \tag{11b}$$

for the amplitude mode (to the order ξ_1^2), with

$$\mathrm{Im} G_0(\mathbf{Q},\omega) \cong \pm \pi \bar{n}_{01} M_1^2 \frac{\Delta_1}{2\omega}$$

times the δ-functions at $\omega = \pm\omega_A$ and $\omega = \pm\omega_P$. Within RPA the modulation of the population difference $n_{01}(i)$ [proportional to γ, see (A1) and (A7) in the Appendix], implies the occurrence of an adiabatic, finite-frequency phason mode at $\mathbf{q} = \pm\mathbf{Q}$. This mode corresponds to a uniform oscillation of the phase u_1 of the modulated structure, except that the adiabatic condition means that the modulation of the population factors stays constant. This condition, in turn, gives rise to the restoring force, which determines the frequency ω_P. The singularity at zero frequency [$\delta_{\omega,0}$ in (A11)] implies the presence of an elastic response. The calculated elastic scattering intensity,

$$I(\mathbf{q},0) = \lim_{\epsilon \to 0} \int_{-\epsilon}^{\epsilon} S(\mathbf{q},\omega) d\omega \ ,$$

is indeed found to diverge corresponding to $\mathrm{Re} G_0(\mathbf{q},0) \to \infty$ for $\mathbf{q} \to \pm\mathbf{Q}$. There is no restoring force acting against a uniform change of the phase u_1 in the incommensurate case, when the change is performed so slowly that thermal equilibrium is maintained. Hence, in the present system there is no well-defined propagating mode ("Goldstone mode") in the limit of $\omega \to 0$ and $\mathbf{q} \to \pm\mathbf{Q}$. Instead we find both a diffusive peak, of diverging intensity, and a phason mode which stays at finite frequency. This contrasts with the behavior of a Goldstone broken-symmetry system (for a discussion see Forster[16]), but is equivalent, within the RPA, to a singlet-triplet system at T_N.

In Figs. 4 and 5 we show the excitation energies for the optical modes propagating in the ΓM direction parallel to $\mathbf{Q}$ (i.e., perpendicular to the pressure axis). The lines show the dispersion relations for both the longitudinal and transverse modes as deduced in the RPA, and the circles denote the peak positions observed by McEwen *et al.*[3-5] The dispersion relation for the transverse mode has been derived in a similar way as for the longitudinal mode except that the $|3_s\rangle$ level has to be included. On the other hand, the off-diagonal couplings, corresponding to $V_{2n\pm 2}(\mathbf{q})$ in (8), lead in this case to energy gaps of the order of only 0.05 meV and can be neglected. We also neglect the low-energy, transverse excitation at energies around $\Delta_2 - \Delta_1$ as the intensity of this mode is extremely weak. For the longitudinal excitations the off-diagonal terms in (8) are important, and they imply the presence of several peaks in the spectrum at most $\mathbf{q}$ values. The most

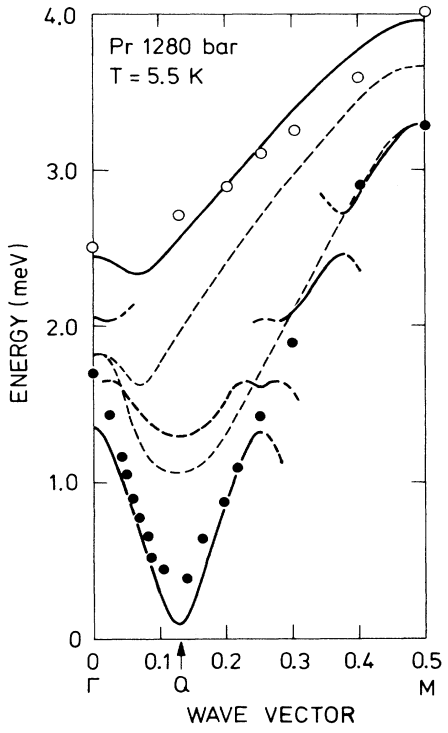

FIG. 4. The dispersion relation of the optical excitations in the antiferromagnetic phase of Pr at 5.5 K under an applied uniaxial pressure of 1280 bars. The ΓM direction considered is the one which is perpendicular to the pressure axis. The circles mark the peak positions obtained in inelastic-neutron scattering experiments (Ref. 3), with solid and open circles indicating the longitudinal and transverse branches, respectively. The solid lines are the calculated RPA energies of the excitations with the largest intensities, whereas the thick dashed lines indicate longitudinal excitations of weaker intensities. The thin dashed lines are the (experimental) dispersion relations in unstressed Pr (Ref. 1) at $T = 6.4$ K, which determine the (effective) exchange parameters, $\mathcal{J}(\mathbf{q})$, used in the calculations.

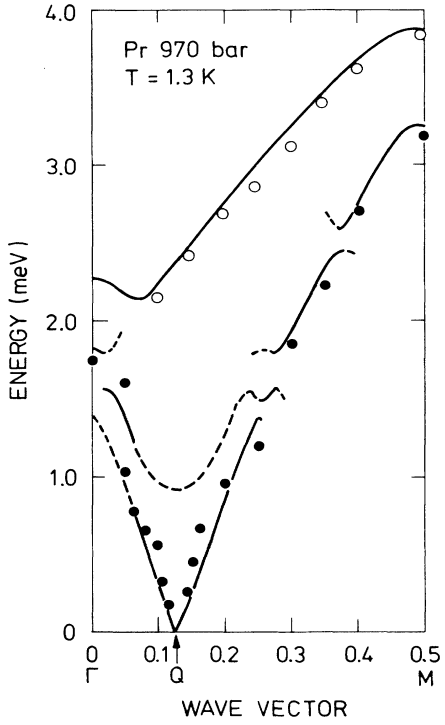

FIG. 5. The same as in the caption to Fig. 4, except that this figure shows the results at 1.3 K with an applied pressure of 970 bars.

intense ones (indicated by solid lines) for $\mathbf{q}$ around $\mathbf{Q}$ are due to the low-lying phason mode, mainly because $\mathrm{Im}G_0(\mathbf{q},\omega)$ is proportional to $1/\omega$ but further enhanced by the detailed-balance factor in $S(\mathbf{q},\omega)$. The low-intensity modes are indicated by thick dashed lines and are not easily detected experimentally. Figure 4 shows the results at $T=5.5$ K and 1280 bars, and, as discussed, the RPA predicts an energy gap which, however, is small for the phason mode. In Fig. 5 the results are shown at 1.3 K and 970 bars. At this low temperature γ is practically zero and the phason energy gap at $\mathbf{Q}$ can be neglected.

In these calculations we have assumed $\mathbf{Q}$ to be an irrational fraction of a reciprocal lattice vector. We have already seen that because $\xi_1 \cong \frac{1}{4}\sigma_1^2 \ll 1$, this assumption plays no role for the linewidth of the excitations. This also hold true for σ_1 and the excitation energies. The differences are general of the order of ξ_1^4, where $\xi_1=0.026$ at $T=0$ and 970 bars. In this case, the phason energy gap, which vanishes in the incommensurate case, is estimated to be 0.030 meV, or very nearly zero, when $\mathbf{Q}$ is commensurate. The calculated spectrum would have appeared almost the same if $\mathbf{Q}$ had been chosen to be $\frac{1}{8}\tau_{100}$. One main reason for assuming the phase to be incommensurate is that the neutron-scattering results clearly indicate a finite linewidth of the excitations, even at the lowest temperatures. Part of an explanation might have been based on an incommensurable ordering of the moments, but we have to consider other possibilities.

IV. LIFETIMES

A. Scattering against single-site fluctuations

In paramagnetic Pr the most important mechanism producing a finite lifetime of the excitations is known to be the fluctuations in the population factors of the single-site levels.[7] This effect appears in the first order of a high-density expansion,[7,17] the $1/z$ expansion [the RPA is obtained in the order $(1/z)^0$], but it is also found by a consideration of the equations of motion.[18] In the ordered phase, which we are considering, the single-site state vectors are only changed slightly in comparison with those occurring in the paramagnetic case, so we anticipate that this mechanism is still the important one. Due to the exchange coupling, the ground state in the paramagnetic regime is not the simple product of the single-site ground states. The situation is entirely equivalent to the Heisenberg antiferromagnet, in which case quantum fluctuations imply that the numerical value of the expectation value of S_z is less than S at $T=0$. Correspondingly, the average value of n_{01}, $\langle n_{01}\rangle \cong 1-3\langle n_1\rangle$, is less than one in the present system at $T=0$. The quantum fluctuations also imply that the number of elementary excitations might change in the scattering processes, leading to damping effects, at finite frequencies, even if $T=0$. However, to first order in $1/z$, the linewidths vanish exponentially like $(1-n_{01}^2)$ in the zero-temperature limit. The equation-of-motion method[18] suggests an estimate of the remaining damping effects via a replacement of the population factors by their self-consistent values, so that the factor $(1-n_{01}^2)$ in the imaginary part of the self-energy is being replaced by $(1-\langle n_{01}\rangle^2)$. This procedure has been applied by Leuenberger and Güdel[19] in an analysis of the magnetic excitations in the dimer system $Cs_3Cr_2Br_9$. The magnetic system of the Cr ions (roughly singlet-triplet but without any dipole matrix elements within the triplet levels) is nearly equivalent to the roughly singlet-doublet case of paramagnetic Pr. Leuenberger and Güdel calculated the line shapes of the excitations at low temperatures. They obtained a reasonable overall agreement with experiment athough the conditions in $Cs_3Cr_2Br_9$ are rather extreme, $\langle n_{01}\rangle \cong 0.81$ in comparison with $\langle n_{01}\rangle \simeq 0.97$ in Pr;[18] both values are at $T=0$. Instead of using this phenomenological approach we shall consider directly the contributions appearing in the second order of the $1/z$-expansion.

Introducing the self-energy $\Sigma(\mathbf{q},\omega)$, the final Green's function may be written

$$G(\mathbf{q},\omega)=\frac{g_0(\omega)}{1-[\mathcal{J}(\mathbf{q})+\Sigma(\mathbf{q},\omega)]g_0(\omega)}, \quad g_0(\omega)=\frac{2\Delta n_{01}}{\Delta^2-\omega^2} . \tag{12}$$

For simplicity we shall only consider here the $S=1$ paramagnet ($M_1=1$ and $\Delta_1=\Delta_2=\Delta$). Neglecting the real part of $\Sigma(\mathbf{q},\omega)$, and the coupling between the J_z components, then $\Sigma(\mathbf{q},\omega)$, in the order $1/z$, is independent of $\mathbf{q}$, and is given by[17]

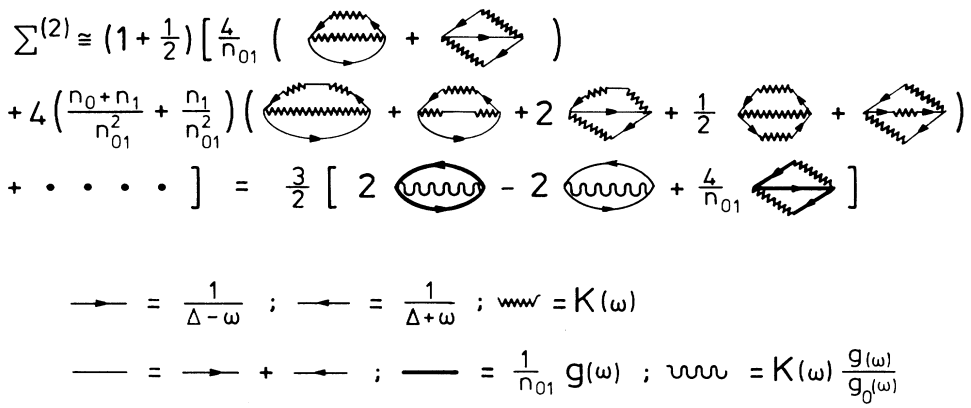

FIG. 6. The diagrammatic representation of the second-order $1/z$ contributions to the single-site self-energy, in the first bracket, plus the corresponding higher-order terms [in "$K(\omega)$"], of which we show the third-order terms in the second bracket. The meaning of the symbols used in the diagrams is also shown. Notice that in the present approximation $g(\omega)$ is given by Eq. (13) using the approximate expression for $\Sigma^{(1)}(\omega)$. Besides the diagrams shown, one should add all equivalent combinations, in which the arrows on lines joining each other are reversed simultaneously.

$$\Sigma^{(1)}(\omega)=i\frac{1}{n_{01}^2}\left[1-n_{01}^2-\frac{\Delta^2-\omega^2}{2\Delta^2}n_1\right]\mathrm{Im}K(\omega)$$
$$\simeq i\left[\frac{1}{n_{01}^2}-1\right]\mathrm{Im}K(\omega) \tag{13a}$$

(the approximate expression only introduces errors of less than 10%). Here $\mathrm{Im}K(\omega)$ is the imaginary part of $K(\omega)$, the effective-medium coupling parameter, which is determined self-consistently in terms of the effective single-site Green's function:[17]

$$g(\omega)\equiv\frac{1}{N}\sum_{\mathbf{q}}G(\mathbf{q},\omega)=\frac{g_0(\omega)}{1-[K(\omega)+\Sigma^{(1)}(\omega)]g_0(\omega)}\ . \tag{13b}$$

Actually, the $1/z$ expansion gives a systematic expansion of

$$g_1(\mathbf{q},\omega)=[1/g_0(\omega)-\Sigma(\mathbf{q},\omega)]^{-1}$$

rather than of $\Sigma(\mathbf{q},\omega)$. However, as shown in Ref. 17, neglecting the higher-order $1/z$ terms in $\Sigma(\mathbf{q},\omega)$, instead of in $g_1(\mathbf{q},\omega)$, leads to a more satisfactory account of the ground-state properties, and the Green's functions behave smoothly around $\omega\cong\Delta$. Here we shall be concerned with only the $(1/z)^2$-terms which contribute to the imaginary part of $\Sigma(\mathbf{q},\omega)$ at low temperatures. Furthermore we neglect terms due to couplings between the J_z components. The latter approximation should be reasonable at low temperatures, and even more so in Pr where the J_z matrix element within the doublet states is relatively small. In addition to the imaginary $(1/z)^2$ terms, which vanish exponentially ($\propto n_1$) for $T\to 0$ and can be neglected in comparison with $\Sigma^{(1)}(\omega)$, there are both single- and two-site terms which depend directly on the thermal population of the dispersive excitonic states. Although these terms are of the order $(1/z)^2$ they might be more important than $\Sigma^{(1)}(\omega)$ at low temperatures if the system contains low-energy excitons. These contributions to the single-site Green's function, $\Sigma^{(2)}(\omega)$ in (13b), are shown in a diagrammatic fashion in Fig. 6. As a simplification, the contributions due to the transverse J_x component are here included approximately by multiplying the longitudinal terms in the squared bracket by the factor $\frac{3}{2}$. This approximation is equivalent to the one made above in Eq. (13a). In Fig. 6 we include also the third- and higher-order diagrams related to the second-order terms considered. When $\Sigma^{(1)}(\omega)$ is added to $\Sigma^{(2)}(\omega)$, $\Sigma^{(1)}(\omega)$ cancels the second term in the sum given in Fig. 6, and according to the diagrams the imaginary part of the self-energy in the single-site Green's function is given by Eq. (14a):

$$\Sigma(\omega)=\Sigma^{(1)}(\omega)+\Sigma^{(2)}(\omega)$$
$$\cong i\frac{3}{2}\frac{1}{4\pi^2 n_{01}^2}\int_{-\infty}^{\infty}d\omega'\int_{-\infty}^{\infty}d\omega''\coth\left[\frac{\beta\omega'}{2}\right]\left[\coth\left[\frac{\beta\omega''}{2}\right]-\coth\left[\frac{\beta(\omega''-\omega)}{2}\right]\right]$$
$$\times\left[\left[1+\frac{1}{\Delta^2}\omega'(\omega'-\omega'')\right]^2 h(\omega')h(\omega'-\omega'')\frac{H(\omega''-\omega)}{g_0(\omega''-\omega)}\right.$$
$$+\frac{2}{n_{01}^2}\left[1+\frac{1}{\Delta^2}\omega'(\omega''-\omega)\right]\left[1-\frac{1}{\Delta^2}(\omega'-\omega'')(\omega''-\omega)\right]$$
$$\left.\times H(\omega')H(\omega'-\omega'')h(\omega''-\omega)\right], \tag{14a}$$

with

$$h(\omega)=\mathrm{Im}g(\omega),\quad H(\omega)=\mathrm{Im}[g(\omega)K(\omega)]\ . \tag{14b}$$

In the order $(1/z)^2$ there are also two-site contributions to $\Sigma(\mathbf{q},\omega)$. However, the averages of these terms with respect to $\mathbf{q}$ are approximately zero, as the corresponding single-site contributions are already included in $\Sigma(\omega)$ via the last two diagrams in Fig. 6 in the bracket containing the third-order terms. Here we shall use an effective-medium approximation, in which we neglect the $\mathbf{q}$-dependent $(1/z)^2$ contributions, $\Sigma(\mathbf{q},\omega)\cong\Sigma(\omega)$. Because of the long range of the interactions this approximation should be reasonable in Pr.

The results above are straightforwardly generalized to the case of the ordered phase as $\Sigma(\omega)$, (14), is just added to $\mathcal{J}(\mathbf{q})$ everywhere. Only, the uniaxial pressure reduces the relative weight of the transversal contributions in Eq. (14) by a factor of 2 ($\frac{3}{2}$ is replaced by $\frac{5}{4}$) below the threshold frequency of the transverse excitations. Besides this, the presence of the ordered moments generates additional terms in the fourth-order semi-invariants which determine the $1/z$ single-site contributions (see Ref. 17, and here we consider the molecular-field Hamiltonian to be the unperturbed one). Neglecting terms of the order σ_1^4, and terms which only contribute to the real part of the self-energy, we obtain the following expression for the $1/z$ contribution to the yy component of the effective single-site Green's function (13b):

$$\delta g_j(\omega)=g_j(\omega)M_1^2\sin^2(2\theta_j)\sum_\alpha[\Xi_\alpha(\omega)-\Xi_\alpha(-\omega)]\ , \tag{15a}$$

where

$$\Xi_y(\omega)=i\frac{\Delta_1}{\omega^2}\frac{\Delta_1+\omega}{\Delta_1-\omega}\left[\coth\left[\frac{\beta(\Delta_1-\omega)}{2}\right]-\coth\left[\frac{\beta\Delta_1}{2}\right]\right]$$

$$\times\mathrm{Im}K_y(\Delta_1-\omega)\ . \tag{15b}$$

Following our previous arguments, $\Xi_z(\omega)$ is negligible in Pr at low temperatures, whereas $\Xi_x(\omega)$, due to the interaction between the x components of the moments, is included (approximately) by multiplying $\Xi_y(\omega)$ with

$$\left[1+\frac{1}{4}\frac{n_2}{n_1}\left[\frac{\Delta_1-\omega}{\Delta_1}\right]^2\right]\ .$$

$\Xi_y(\omega)$ diverges like $1/\omega$ in the limit $\omega\to0$ indicating that $\delta g_j(\omega)$ affects the behavior of the diffusive peak. This divergence is removed if ω^2 in the denominator of (15b) is replaced by $\omega^2+\Gamma^2$ after having determined Γ from

$$\delta g_j(\omega\to0)=i\frac{\Gamma}{\omega}g^0_{\mathrm{el},j}\ ,$$

where $g^0_{\mathrm{el},j}$ is the elastic contribution in (6) to the noninteracting Green's function. Neglecting a minor term $(4n_0n_1+n_0n_2\simeq n_0+n_1-n_{01}^2)$ we get

$$\Gamma\simeq\frac{2M_1^2}{n_{01}}\mathrm{Im}K_y(\Delta_1)\ . \tag{16a}$$

With this result for the imaginary part, the Kramers-Kronig relation implies that the real part of $g_j(\omega)$ is also modified, namely that the elastic term $g^0_{\mathrm{el},j}$ in (6) is changed into a Lorentzian of width 2Γ:

$$g^0_{\mathrm{el},j}\to\frac{\Gamma^2}{\Gamma^2+\omega^2}\beta(n_0+n_1-n_{01}^2)_jM_1^2\sin^2(2\theta_j)\ . \tag{16b}$$

These results are in accordance with the $(1/z)^2$ contributions, which lead to a replacement of $g^0_{\mathrm{el},j}+\delta g_j(\omega)$ by an integral involving products of two Lorentzians (centered at Δ_1 and $\Delta_1\pm\omega$) both with the width Γ, which Lorentzians are approximately the spectral density of states, proportional to $\mathrm{Im}g(\omega')$. Corresponding to (14) there are other frequency dependent factors in the integral, however, in the present case the additional $(1/z)^2$ modifications have only minor effects on the final results.

The third-order semi-invariants, $\langle J_\alpha(\tau_1)J_\beta(\tau_2)J_\gamma(\tau_3)\rangle$ also appear in the order $1/z$, but only in the two-site Green's function. Hence these contributions are proportional to

$$\sim\frac{1}{N}\sum_{\mathbf{q}'}\mathcal{J}(\mathbf{q}')\mathcal{J}(\mathbf{q}'-q)$$

which reduces their importance, especially in systems with long-range coupling, like in Pr. In the paramagnetic case only the semi-invariant with $(\alpha\beta\gamma)=(xyz)$ is nonzero, and is without any importance in Pr because it involves J_z. The corresponding $\mathbf{q}$ average of the contributions proportional to σ_1^2 was included in our estimate of the second-order contributions to (15a)–(16b), which we found to be unimportant. Because of this, and also because of the great complexity introduced in the numerical analysis, the $\mathbf{q}$-dependent contributions are neglected.

B. Conduction electron scattering

We now consider lifetime effects due to the scattering against electron-hole pair excitations of the conduction electrons. These contributions can be obtained by using the method of Becker *et al.*,[20] however, it is straightforward to incorporate them into the $1/z$ expansion. The Hamiltonian for the interaction between the conduction electron spin $\mathbf{S}$ and the localized angular momentum is assumed to be

$$H_{\mathrm{sf}}=-2I_0\sum_n\mathbf{J}_n\cdot\mathbf{S}(\mathbf{r})f(\mathbf{r}-\mathbf{R}_n)\ . \tag{17}$$

This Hamiltonian leads to the usual Ruderman-Kittel-Kasuya-Yosida (RKKY) coupling of the angular momenta, but because of retardation effects the interaction also includes an imaginary term, and hence $\mathcal{J}(\mathbf{q})$ is replaced by

$$\mathcal{J}(\mathbf{q})\to\mathcal{J}(\mathbf{q})+i\omega\zeta(\mathbf{q})\ , \tag{18a}$$

with

$$\zeta(\mathbf{q})=\pi|N(0)I_0|^2\frac{2}{3n}\sum_\tau^{|\mathbf{q}+\tau|<2k_F}\frac{k_F}{|\mathbf{q}+\tau|}|f(\mathbf{q}+\tau)|^2 \tag{18b}$$

when assuming a free-electron-like behavior of the con-

duction electrons. $N(0)$ is the density of states at the Fermi surface (per atom and per spin state), k_F is the Fermi wave vector ($\simeq 1.4$ Å^{-1}), n ($=3$) is the number of conduction electrons per atom, τ denotes a reciprocal lattice vector, and $f(\mathbf{q}+\tau)$ is the form factor of the $4f$ electrons. In the case of Pr, the limited importance of the moments on the cubic sites on the magnetic properties at low energies implies, roughly speaking, that the coupling between the two sublattices should be subtracted in (18), which in (18b) gives rise to a factor $\frac{1}{2}$ plus a doubling of the number of reciprocal lattice vectors. It is important to note that this also means that the effective $\mathcal{J}(\mathbf{q})$ is no longer simply proportional to the susceptibility of the conduction electrons, in contrast to, for instance, the (hcp) heavy rare-earth metals.

The replacement made in (18a) can be incorporated directly in the diagrammatic $1/z$ expansion just by including the imaginary term in the interpretation of the bare interaction lines. Then to zero order in $1/z$ (i.e., RPA) the self-energy (12) is $\Sigma^{(0)}(\mathbf{q},\omega)=i\omega\zeta(\mathbf{q})$. To next order in $1/z$, the effects of the electron-hole pair excitations on the single-site fluctuations may be obtained (approximately) by substituting the average value $i\omega\zeta_0=i\omega\langle\zeta(\mathbf{q})\rangle$ for $K(\omega)$ in (13a). These are the contributions also considered by Becker *et al.*[20] (for arbitrary values of S). In the $S=1$ case the two methods lead to equivalent results, also when considering the effect on the diffusive peak in the ordered phase (16). However, there are "higher-order" differences, and the $1/z$ classification of the terms seems a more satisfactory approach. The present procedure enables the two types of contribution to the self-energy to be combined readily, with the result that in all the expressions deduced previously $K(\omega)$ should be replaced by

$$\hat{K}(\omega)=K(\omega)+i\omega\zeta_0 , \tag{19a}$$

and $\Sigma(\mathbf{q},\omega)$ is then given by

$$\Sigma(\mathbf{q},\omega)=\hat{\Sigma}(\omega)+i\omega\zeta(\mathbf{q}) , \tag{19b}$$

where $\hat{\Sigma}(\omega)$ is the modified result for $\Sigma(\omega)$. The average value $\zeta_0\cong 2\pi\,|N(0)I_0|^2\,|f(2k_F)|$ determines the magnetic contribution, λ_{em}, to the enhancement factor of the linear term in the electronic heat capacity,[21] since $2\pi N(0)\lambda_{em}=\zeta_0\chi_0$, where $\chi_0\cong 8.1$ meV^{-1} is the mean of the static susceptibility. Using[22] $N(0)=0.66$ eV^{-1} (per atom and spin state) the heat capacity measurements[23] yield a value of $\lambda_{em}=3.8\pm 0.3$ (assuming a finite temperature enhancement of the experimental λ_{em} of about 17%, see Fig. 2 of Ref. 21, and a phonon contribution[22] $\lambda_{ep}=1.1$) and thus $\zeta_0=(1.9\pm 0.2)10^{-3}$. In the low-temperature experiments on Pr (Ref. 1) effects due to $\zeta(\mathbf{q})$, (19b), were detected, but only for the acoustic modes at small wave vectors, $q<0.3$ Å^{-1}, indicating that $\zeta(\mathbf{q})$ at large wave vectors must be smaller than $\sim 3\times 10^{-3}$. Various estimates, utilizing (18b) combined with the above value for ζ_0, or based on the extrapolation of the experimental values of $\zeta(\mathbf{q})$, indicate consistently that for the optical modes $\zeta(\mathbf{q}\approx\mathbf{Q})\approx 2.0\times 10^{-3}$, corresponding to a linewidth of ~ 0.15 meV in agreement with recent measurements on unstressed Pr and Pr + 2.5% La. This value has been employed in the following analysis.

C. Comparison with experiments

In order to compare with experiment, we calculated the correlation function for different temperatures and wave vectors in the presence of an applied pressure of 970 bars. In the calculation of $\Sigma(\omega)$, (14), a number of simplifications were necessary contributing an overall error of roughly 10—20%, which is comparable with other unavoidable uncertainties in the numerical analysis.

In the optical, low-frequency part of the spectrum the paramagnetic contribution, (14), is the dominating term in the calculated linewidths except at temperatures below ~ 5 K. In comparison with the first-order contribution, the second-order term is of considerable importance at all the temperatures considered. $\Sigma(\omega)$ varies much more smoothly than $\Sigma^{(1)}(\omega)$ both with respect to frequency and temperature. Whereas $\Sigma^{(1)}(\omega)$ decreases exponentially at low temperatures, and is negligible $\lesssim 7$ K, $\Sigma^{(2)}(\omega)$ contributes even at $T=0$. However, the linewidths due to $\Sigma^{(2)}(\omega)$ at $T=0$ are small (~ 0.02 meV at energies of ~ 1 meV) and they vanish for $\omega\to 0$. It is worth pointing out that $\Sigma^{(2)}(\omega)$ is nonzero also outside the RPA excitonic band, and, for instance, just above T_N, $\Sigma^{(2)}(\omega)$ predicts an appreciable low energy scattering at the ordering wave vector, leading to a diffusive behavior of the critical mode, near the transition, instead of the soft-mode behavior predicted to zero or first order in $1/z$. Below about 5 K the electron-hole pair scattering is calculated to be the dominant term in $\Sigma(\mathbf{q},\omega)$. It is the zero-order term $i\omega\zeta(\mathbf{q})$ which is the important one as it adds a contribution of about 0.15 meV to the calculated linewidths, nearly independently of the temperature. The higher-order effects introduced by substituting $\hat{K}(\omega)$ for $K(\omega)$, (19a), have only the minor consequence that $\hat{\Sigma}(\omega)$ is enhanced 10—20% in comparison with $\Sigma(\omega)$.

In the ordered phase the most important modifications produced by the moment fluctuations, (15), occur at the lowest frequencies close to $\mathbf{Q}$. The width of the Lorentzian diffusive peak in the single-site response function, 2Γ in (16), is found to be large. $\pi n_{01}M_1^2\mathrm{Im}K_y(\Delta_1)\simeq\mathcal{N}_y^{-1}(\Delta_1)$, where $\mathcal{N}_y(\omega)$ is the density of excitonic y modes, leads to $\Gamma\simeq 0.9$ meV at low temperatures, a value which is increased by 15% due to the electron-hole pair scattering mechanism. This large width implies that the RPA prediction of an inelastic phason mode at $\mathbf{q}=\mathbf{Q}$, as indicated in Fig. 4, does not hold true. As long as $\mathbf{q}$ is close to $\mathbf{Q}$ we are left with only a diffusive peak of finite width; there is no extra maximum in the correlation function at nonzero frequencies below that of the amplitude mode. Defining δq to be the distance away from $\mathbf{Q}$ where an inelastic peak does appear at the lowest frequencies, then δq, along τ_{100} at the pressure of 970 bars, is calculated to be $0.027\,|\tau_{100}|$ at 7.1 K. When the experimental energy resolution is included, δq is increased to be about $0.035\,|\tau_{100}|$ in fair agreement with the observations.[6] δq is predicted to vanish at $T\equiv 0$ but to be still about $0.01\,|\tau_{100}|$ at 1.3 K. The damping of the diffusive broken-symmetry mode is related to the circumstance that the Hamiltonian does not commute with the generator of an infinitesimal shift in the phase of the order parameter, $1+i\delta\theta\sum_j(|1_a\rangle\langle 1_a|)_j$, in accordance with the discus-

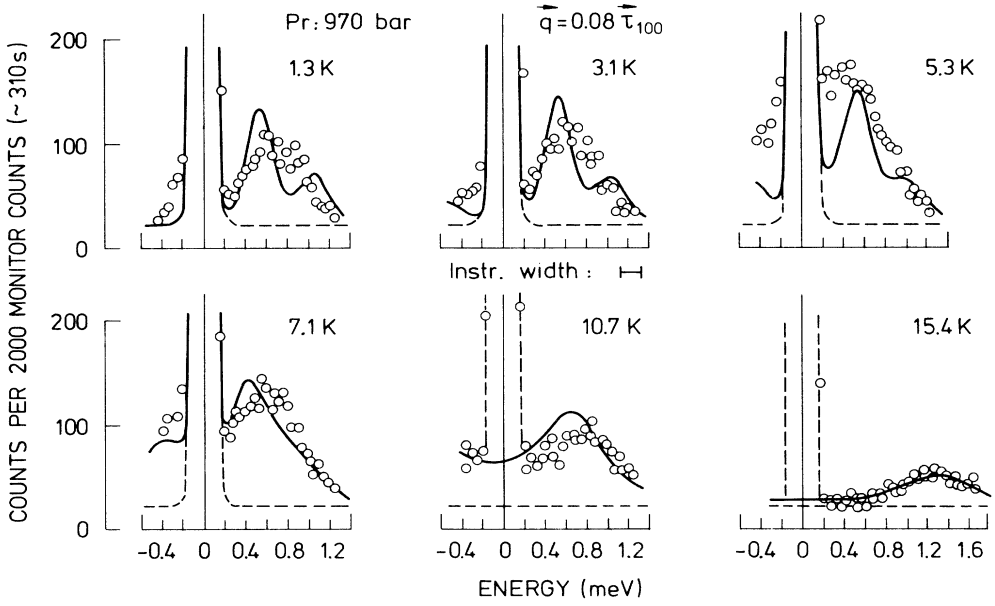

FIG. 7. The total numbers of inelastic scattered neutrons (Ref. 3) counted in constant $\mathbf{q}$ scans, $\mathbf{q}=0.08\tau_{100}$, in Pr at various temperatures, under a uniaxial pressure of 970 bars. The solid lines are the calculated scattering functions convoluted with the instrumental resolution function of the width (FWHM) shown in the figure, to which we have added the background scattering indicated by the dashed lines.

sion of Zeyher and Finger.[24] As expected the half width of the diffusive peak tends to zero when $\mathbf{q}\rightarrow\mathbf{Q}$. More accurately, it is the maximum intensity which diverges, as the theory predicts that a strong inelastic tail remains at $\mathbf{q}=\mathbf{Q}$. This unusual feature may be considered as a remnant of the adiabatic phason mode at $\mathbf{q}=\mathbf{Q}$ predicted by the RPA.

The diffusive mode may be of some importance for explaining *elastic* neutron scattering experiments.[6] It will give rise to a Gaussian-like peak centered at $\mathbf{Q}$, overlying

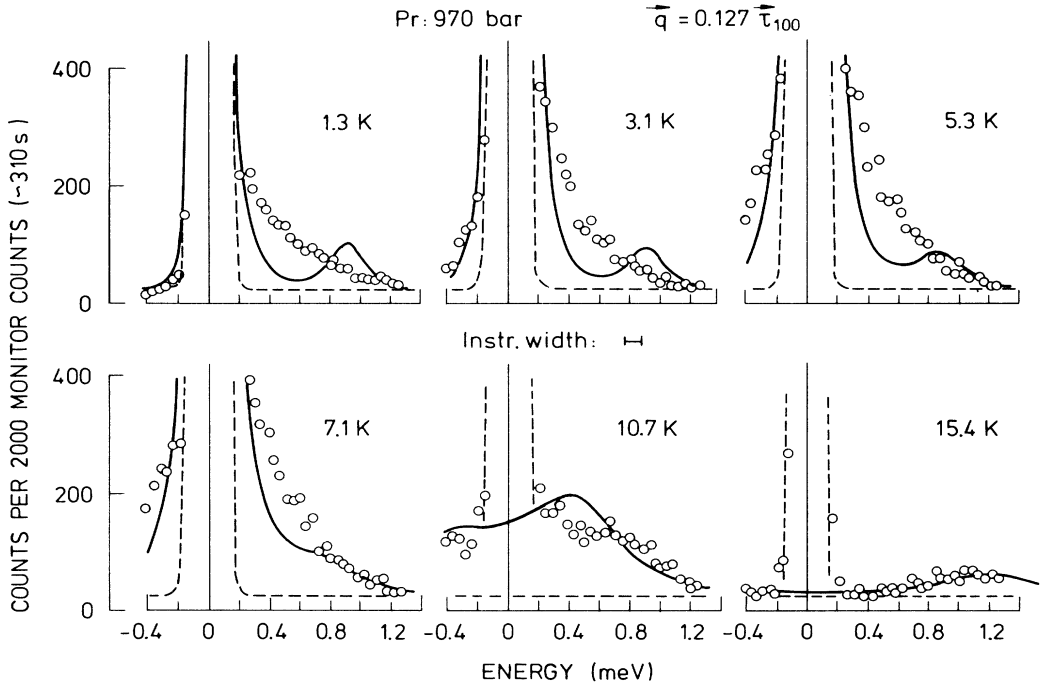

FIG. 8. The same as in Fig. 7 when $\mathbf{q}=0.127\tau_{100}$, close to the ordering wave vector.

the magnetic Bragg peak. The full width at half maximum (FWHM) of this extra peak is calculated to be about $0.01\,|\tau_{100}|$ for $\mathbf{q}$ along τ_{100}. The intensity vanishes linearly with T at low temperatures, and the peak disappears above T_N. A comparison with the intensity of the Bragg peak depends sensitively on the instrumental resolution function. However, including most of the integrated intensity of the diffusive mode, it is estimated to be of the order of one third of the magnetic Bragg peak at temperatures around 7 K.

In Figs. 7 and 8 are shown the comparisons between the calculated and experimental neutron scattering intensities, at various temperatures both above and below T_N, for two different wave vectors. One is $\mathbf{q}=0.08\tau_{100}$, which is representative for the cases where $\mathbf{q}$ is not close to $\mathbf{Q}$, and the other is $\mathbf{q}=0.127\tau_{100}$, or in practice equal to $\mathbf{Q}$. The calculated correlation functions have been convoluted with the experimental resolution function, assumed to be a Gaussian. At $\mathbf{q}=0.08\tau_{100}$ the instrumental width of the Gaussian was established from a measurement of the incoherent scattering from vanadium. In the other case, $\mathbf{q}=0.127\tau_{100}$, we use an instrumental width of about $\frac{2}{3}$ times the one determined experimentally in order to fit the negative energy tail of the Bragg peak at 1.3 K (this narrowing of the width is expected and arises from the very rapid $\mathbf{q}$ dependence of the elastic intensity). The only fitting parameter of importance for the comparison is the intensity scale. If focusing effects are neglected, the scale parameter should be independent of temperature, and it should be about the same at the two different wave vectors. Accordingly, we use the same scale parameter in all the cases shown in the two figures.

At both wave vectors there is a good agreement between the calculated and the experimental inelastic scattering intensities, both in the paramagnetic phase ($T_N \simeq 9.7$ K) and at the highest temperatures in the ordered phase (notice that σ_1 is already about 85% of the zero-temperature value at 7.1 K). At the two lowest temperatures the calculation predicts a more clear manifestation of the amplitude mode than seen experimentally. At $\mathbf{q}=0.08\tau_{100}$ most of the discrepancies might be removed if the amplitude mode is shifted downwards in energy by about ~ 0.2 meV, an effect which might be produced by the contributions to the real part of $\Sigma(\mathbf{q},\omega)$ neglected in the present calculation. A shift in energy of the amplitude mode is not sufficient to account for the discrepancies at the lowest temperatures when $\mathbf{q}=0.127\tau_{100}$. Nevertheless, the most important feature, the large inelastic intensities observed all the way down to the tail of the elastic scattering, agree in order of magnitude with the predictions in the ordered phase. This agreement, and also the consistency between the calculated values of δq and the observations which we discussed above, must be considered as an experimental verification of the predicted diffusive behavior of the phason mode.

Below ~ 5 K the discrepancies in Fig. 8 indicate that $\mathrm{Im}\Sigma(\mathbf{q}\simeq\mathbf{Q},\omega)$ is significantly larger than the zero-order term due to the electron-hole pair scattering. It might be possible that terms of higher order than $(1/z)^2$ start to be important at the lowest temperatures, where the second-order terms are small. However, in the perturbative $1/z$ expansion, which is based on the assumption of a unique, well-defined many-body ground state, the linewidth effects are bound to vanish in the zero frequency limit at $T=0$, so the higher-order effects, and also the second-order $\mathbf{q}$-dependent terms which we have neglected, are expected to be of only minor importance at the low frequencies considered here. Another possibility is that the discrepancies might be due to the observed quasielastic peak,[3,4,9,25] of finite width in $\mathbf{q}$ space and centered at a wave vector $\mathbf{Q}^*=0.113\tau_{100}$ (at 970 bars) differing from $\mathbf{Q}$. This broad peak appears at temperatures well above T_N, and the peak intensity seems to be still increasing in the ordered phase. It is the dominating contribution to the zero-energy response at $\mathbf{q}=0.08\tau_{100}$, shown in Fig. 7. The neutron scattering results indicate that the peak is very narrow in ω, and an upper limit on the width has been estimated to lie around 0.1 meV. A comparison[26] between heat capacity measurements and neutron scattering experiments, performed on unstressed Pr in the temperature range 50 mK—5 K, can be interpreted in terms of the nuclear spins being influenced by the quasielastic peak as if it were a diffusive mode of the localized moments. In such a case the width would be smaller than ~ 0.01 meV at the lowest temperatures. The extra contribution to the (nuclear) heat capacity is accounted for by the specific model, but there might be other ways of relating it to the presence of the quasielastic peak. In fact, the indications are that the quasielastic peak is not a dynamic mode involving the localized angular momenta. If this had been the case we might expect a similar phenomenon in the equivalent system $Cs_3Cr_2Br_9$, but this is not observed.[27] The maximum of the response should occur at least very close to $\mathbf{Q}$. Finally, we would expect broadening effects like those observed for the diffusive phason mode. Although the quasielastic peak might be responsible for the low-temperature discrepancies in Fig. 8, these are small effects when compared with the large intensity of the peak. At $\mathbf{q}=0.08\tau_{100}$ a broadening of the peak would have washed out completely the inelastic resonance. These circumstances leave only two possibilities: either the peak is due to static short-range ordered arrangements of the local moments, or it is a magnetic response of the itinerant electrons. The first possibility is discussed in a previous paper,[25] and is concluded to be very improbable. It seems therefore likely that it is the conduction electrons which are responsible for the quasielastic peak. A magnetic scattering like this is not expected from ordinary band electrons, but it might originate from resonance states near the Fermi surface due to a weak hybridization of the conduction electrons with the $4f$ electrons. Because the susceptibility of the conduction electrons does not need to have its maximum at $\mathbf{Q}$ (see the preceding section) $\mathbf{Q}^*$ may differ from $\mathbf{Q}$ in this case. The occurrence of the quasielastic peak might imply that Pr metal is a kind of heavy-fermion system,[28] whose large specific heat is obscured by the very large nuclear contribution.[26]

In the paramagnetic phase near T_N, the experiments[3,4,9] show a strong precursor of the Bragg peak besides the quasielastic peak at $\mathbf{Q}^*$. This is the dominant contribution to the (nearly) elastic scattering indicated by the dashed lines in Fig. 8 at 10.7 K (but not at 15.4 K where

it is a genuine background of incoherent scattered neutrons). This critical phenomenon appears in the theory but only much closer to T_N. An enhancement of the critical scattering might be indicating that the surface is overcritical above T_N, as analyzed by Murao.[29]

V. CONCLUSION

A number of the static and dynamic properties of Pr, in its ordered phase induced by an applied uniaxial pressure, have been explained. The agreement between the calculated predictions and the neutron scattering results is quite satisfactory, especially when considering that the calculations are based exclusively on parameters determined otherwise from experiments on paramagnetic Pr. In the ordered phase the length of the moments is modulated sinusoidally with a period of about eight lattice spacings. This complicates the analysis, but Pr is a singlet ground-state system, and the induced moments below T_N stay small, which allows a perturbative approach with the relative magnetization σ_1 as the expansion parameter. One important consequence of the smallness of σ_1 is, according to our analysis, that the question of whether the ordering wave vector $\mathbf{Q}$ is commensurate or not has nearly no implications on the behavior of the system.

In order to account for the finite linewidths of the excitations we find it to be important to include the contributions of second order in the high-density $1/z$ expansion. These contributions are larger here than in unstressed Pr, because the excitonic density of states is shifted downwards in frequency. In our account of the second-order terms we utilized an effective-medium approximation replacing the self-energy $\Sigma(\mathbf{q},\omega)$ with its average with respect to $\mathbf{q}$. This approximation is justified by the long range of the interaction in Pr. In contrast to the first-order contributions, the second-order linewidths remain finite, although small, in the zero-temperature limit. The introduction of the second-order terms also leads to a qualitative improvement in the description of the phase transition, by transforming the incipient soft mode into a diffusive mode just above T_N.

Because of the smallness of the intrinsic contributions to $\Sigma(\mathbf{q},\omega)$ at the lowest temperatures, the scattering of the excitons against electron-hole pair excitations of the conduction electrons starts to become important. Instead of using the theory of Becker, Fulde, and Keller,[20] this external scattering mechanism was incorporated in the $1/z$ expansion calculations, allowing a direct comparison with the intrinsic effects. This showed that, in the present system, the intrinsic effects caused by the single-site fluctuations are much larger than the additional effects introduced by the electron-hole pair scattering, leaving only the terms of zero order in $1/z$, which is unique for the electron-hole pair scattering mechanism, to be of any importance. The magnitude of this term was estimated and it gives rise to linewidths of about 0.15 ± 0.05 meV at the wave vectors considered.

The broken-symmetry mode, i.e., the phason mode, is predicted not to be a propagating Goldstone mode whenever $T>0$. At wave vectors close to $\mathbf{Q}$ the phason mode is diffusive, and damped because of the fluctuations of the ordered moments. Most unusually there remain inelastic tails on the sides of the diverging elastic peak of the phason mode at $\mathbf{Q}$. The predicted linewidth phenomena, and also the behavior of the phason mode agree in many details with the experiments. There are qualitative discrepancies of some significance, but only below ~ 5 K when $\mathbf{q}$ is close to $\mathbf{Q}$.

The nature of the quasielastic peak in Pr, centered at a wave vector $\mathbf{Q}^*$ different from $\mathbf{Q}$, has been further elucidated in the present work, utilizing the fact that the low-frequency excitations in the ordered phase probe the dynamic response connected to this peak. In relation to its large intensity the dynamic effects, which may possibly be associated with the quasielastic peak, are very modest. Because it is unlikely that it is a static phenomenon due to the localized $4f$ moments, it seems probable that it is a response coming from the itinerant spins and, hence, a resonance phenomenon due to a weak delocalization of the $4f$ electrons.

ACKNOWLEDGMENTS

One of us (J.J.) gratefully acknowledges the hospitality of the Institut Laue-Langevin where part of this work was done. The experiments discussed in this paper were carried out in collaboration with C. Vettier. We have benefited greatly from discussions with him and with T. A. L. Ziman, R. Micnas, and A. R. Mackintosh.

APPENDIX

The MF equations, (2)–(4), can be solved analytically, within the effective $S=1$ model, using σ_1 as an expansion parameter. Below T_N the population difference $n_{01}(i)$ in Eq. (3) is site dependent, since the energy splittings between the MF levels are modulated such that $\Delta_1(i)=\Delta_i/\cos(2\theta_i)$, whereas Δ_2 and Δ_3 are changed by $[1/\cos(2\theta_i)-1]\Delta_1/2$. The expansion of the population factor to second order in θ_i is written

$$n_{01}(i)=\bar{n}_{01}[1+\gamma\cos(2\mathbf{Q}\cdot\mathbf{R}_i+2u_1)]\ . \tag{A1}$$

Introducing

$$\theta_i=\phi_1\cos(\mathbf{Q}\cdot\mathbf{R}_i+u_1)+\phi_3\cos(3\mathbf{Q}\cdot\mathbf{R}_i+3u_1)\ , \tag{A2}$$

then to leading order in the parameter γ

$$\phi_1^2=\xi_1\left[1-\frac{1}{3}\frac{\xi_1}{\xi_3}-\frac{5}{6}\xi_1\right]+\frac{1}{3}\gamma\left[1-\frac{1}{3}\xi_1+\frac{2}{3}\frac{\xi_1}{\xi_3}\right]+O(\sigma_1^6) \tag{A3}$$

and

$$\phi_1\phi_3=\frac{1}{3}\xi_1\left[\frac{\xi_1}{\xi_3}-\gamma-\frac{1}{3}\frac{\gamma}{\xi_3}\right]+O(\sigma_1^6)\ , \tag{A4}$$

where

$$\xi_n=\frac{2\bar{n}_{01}M_1^2\mathcal{J}(n\mathbf{Q})-\Delta_1}{\bar{n}_{01}M_1^2\mathcal{J}(n\mathbf{Q})+\Delta_1}\ . \tag{A5}$$

The first harmonic of the relative magnetization is found

to be given by

$$\sigma_1=\frac{3\bar{n}_{01}\Delta_1}{\bar{n}_{01}M_1^2\mathcal{J}(\mathbf{Q})+\Delta_1\left[1-\frac{\gamma}{2}\right]}\phi_1+O(\sigma_1^5)\ . \tag{A6}$$

γ is proportional to ξ_1 ($\beta=1/k_BT$):

$$\gamma=\frac{1}{2}\frac{1}{\bar{n}_{01}}(\bar{n}_0+\bar{n}_1-\bar{n}_{01}^2)\beta\Delta_1\left[1+\frac{1}{3}\frac{\xi_1}{\xi_3}+\frac{5}{6}\xi_1\right]\xi_1\ , \tag{A7}$$

but because of the population factor in front, γ is an order of magnitude (at least) smaller than ξ_1 in the temperature regime we are considering, and we therefore neglect terms of the order γ^2. At the lowest temperatures, when $\beta\Delta_1\xi_1\gtrsim 1$, the expansion of $n_{01}(i)$ in powers of θ_i is not well behaved. We have included the leading order modification of the results due to this breakdown of the simple expansion by replacing all the zero-order population factors with their mean values, as denoted by the bars, using

$$\frac{1}{2\pi}\int_0^{2\pi}\exp[-\beta(\bar{\Delta}_\alpha+\delta_\alpha\cos u)]du=J_0(z=i\beta\delta_\alpha)e^{-\beta\bar{\Delta}_\alpha}\ , \tag{A8}$$

where $J_n(z)$ are Bessel functions.

The RPA equations of motion for determining $G_{2n}(\mathbf{q},\omega)$, Eq. (8), are derived by multiplying Eq. (5) with the site-dependent energy denominator of $g_i^0(\omega)$. The different terms are then expanded in powers of θ_i. To the same accuracy as the ground state is determined, the parameters in Eq. (8) are

$$E_{2n}(\mathbf{q})=\Delta_1^2\lambda_1-2\Delta_1\bar{n}_{01}M_1^2\mathcal{J}(\mathbf{q}+2n\mathbf{Q})\lambda_2\ , \tag{A9}$$

$$V_{2n}(\mathbf{q})=\Delta_1^2\lambda_3-2\Delta_1\bar{n}_{01}M_1^2\mathcal{J}(\mathbf{q}+2n\mathbf{Q})\lambda_4\ , \tag{A10}$$

with

$$\begin{aligned}
\lambda_1&=1+2\xi_1\left[1-\frac{1}{3}\frac{\xi_1}{\xi_3}+\frac{7}{6}\xi_1\right]+\frac{2}{3}\gamma\left[1+\frac{2}{3}\frac{\xi_1}{\xi_3}+\frac{11}{3}\xi_1\right],\\
\lambda_2&=1-\xi_1\left[1-\frac{1}{3}\frac{\xi_1}{\xi_3}-\frac{13}{12}\xi_1\right]-\frac{1}{3}\gamma\left[1+\frac{2}{3}\frac{\xi_1}{\xi_3}+\frac{2}{3}\xi_1\right]\\
&\quad+2\gamma(1+2\xi_1)\delta_{\omega,0}\ ,\\
\lambda_3&=\xi_1\left[1+\frac{1}{3}\frac{\xi_1}{\xi_3}+\frac{11}{6}\xi_1\right]+\frac{1}{3}\gamma(1+3\xi_1)\ ,\\
\lambda_4&=-\frac{1}{2}\xi_1\left[1+\frac{1}{3}\frac{\xi_1}{\xi_3}-\frac{7}{6}\xi_1\right]+\frac{1}{3}\gamma\\
&\quad+\gamma\left[1+\frac{2}{3}\frac{\xi_1}{\xi_3}+\frac{8}{3}\xi_1\right]\delta_{\omega,0}\ ,
\end{aligned} \tag{A11}$$

where

$$\delta_{\omega,0}=\lim_{\epsilon\to 0}[i\epsilon/(\omega+i\epsilon)]\ .$$

These higher-lying $J=4$ levels of the hexagonal ions not shown in Fig. 1 are of some importance for establishing the $S_{\text{eff}}=1$ parameters used above for calculating σ_1 and the excitation energies. It is, however, not obvious that the $S_{\text{eff}}=1$ calculation is an acceptable approximation. In fact, the presence of the higher-lying levels modifies the molecular field, leading to an increase of the calculated magnetization of about 8%. This result is shown by the solid line in Fig. 3. Due to the larger value of σ_1 the modulation of the crystal-field splittings (or ϕ_1) should increase, but this increase is opposed, and very nearly cancelled, by the coupling between the excited levels induced by the molecular field. So the only modification due to the higher lying levels is the increase of σ_1, in comparison with (A6), whereas the excitation energies are still determined by the expressions above (the corrections are only of the order of 10^{-3} meV).

*Present address: Department of Physics, Birkbeck College, University of London, Malet Street, London WC1E 7HX, U.K.

[1]J. G. Houmann, B. D. Rainford, J. Jensen, and A. R. Mackintosh, Phys. Rev. B **20**, 1105 (1979).

[2]K. A. McEwen, W. G. Stirling, and C. Vettier, Phys. Rev. Lett. **41**, 343 (1978).

[3]K. A. McEwen, W. G. Stirling, and C. Vettier, in *Crystalline Electric Field Effects in f-Electron Magnetism*, edited by R. P. Guertin, W. Suski, and Z. Zolnierek (Plenum, New York, 1982), p. 57.

[4]K. A. McEwen, W. G. Stirling, and C. Vettier, J. Magn. Magn. Mater. **31-34**, 599 (1983).

[5]K. A. McEwen, W. G. Stirling, and C. Vettier, Physica **120B**, 152 (1983).

[6]W. G. Stirling and K. A. McEwen, in *Multicritical Phenomena*, edited by R. Pynn and A. T. Skejltorp (Plenum, New York, 1984), p. 213.

[7]P. Bak, Phys. Rev. Lett. **34**, 1230 (1975); Phys. Rev. B **12**, 5203 (1975).

[8]K. A. McEwen and W. G. Stirling, J. Phys. C **14**, 157 (1981).

[9]H. Bjerrum Møller, J. Z. Jensen, M. Wulff, A. R. Mackintosh, O. D. McMasters, and K. A. Gschneidner, Jr., Phys. Rev. Lett. **49**, 482 (1982).

[10]K. A. McEwen, W. G. Stirling, C. Vettier, J. L. Ragazzoni, D. Fort, and D. W. Jones, Physica **107B**, 259 (1981).

[11]B. Lebech, J. Appl. Phys. **52**, 2019 (1981).

[12]K. A. McEwen, E. M. Forgan, H. B. Stanley, J, Bouillot, and D. Fort, Physica **130B**, 360 (1985).

[13]E. M. Forgan, J. Phys. F **12**, 779 (1982).

[14]Actually, $G_0(\mathbf{q},\omega)$ becomes quite insensitive to the values substituted for $Z_{\pm 2n}$ if n is very large ($n>100$ for $\xi_1\approx 1$), and if ω is being shifted slightly away from the real axis, e.g., $\omega=\omega_1+i\omega_2$ with $\omega_2=0.01\omega_1$. The present procedure merely leads to a reproduction of the correlation function calculated by Ziman and Lindgård (Ref. 15).

[15]T. Ziman and P. A. Lindgård, Phys. Rev. B **33**, 1976 (1986); and (private communication).

[16]D. Forster, *Hydrodynamic Fluctuations, Broken Symmetry, and Correlation Functions* (Benjamin, London, 1975).

[17]J. Jensen, J. Phys. C **17**, 5367 (1984).
[18]J. Jensen, J. Phys. C **15**, 2403 (1982).
[19]B. Leuenberger and H. U. Güdel, J. Phys. C **18**, 1899 (1985).
[20]K. W. Becker, P. Fulde, and J. Keller, Z. Phys. B **28**, 9 (1977).
[21]P. Fulde and J. Jensen, Phys. Rev. B **27**, 4085 (1983).
[22]M. Wulff, G. G. Lonzarich, and H. Skriver (unpublished).
[23]E. M. Forgan, Physica B **107**, 65 (1981).
[24]R. Zeyher and W. Finger, Phys. Rev. Lett. **49**, 1833 (1982).
[25]S. K. Burke, W. G. Stirling, and K.A. McEwen, J. Phys. C **14**, L967 (1981).
[26]M. Eriksen, E. M. Forgan, C. M. Muirhead, and R. C. Young, J. Phys. F **13**, 929 (1983).
[27]B. Leuenberger, H. U. Güdel, R. Feile, and J. K. Kjems, Phys. Rev. B **31**, 597 (1985).
[28]N. d'Ambrumenil and P. Fulde, J. Magn. Magn. Mater. **47&48**, 1 (1985).
[29]T. Murao, Prog. Theor. Phys. **80**, Suppl., 139 (1984).